



## High downforce race car vertical dynamics: aerodynamic index

Felipe Pereira Marchesin, Roberto Spinola Barbosa, Marco Gadola & Daniel Chindamo

To cite this article: Felipe Pereira Marchesin, Roberto Spinola Barbosa, Marco Gadola & Daniel Chindamo (2017): High downforce race car vertical dynamics: aerodynamic index, Vehicle System Dynamics, DOI: [10.1080/00423114.2017.1413196](https://doi.org/10.1080/00423114.2017.1413196)

To link to this article: <https://doi.org/10.1080/00423114.2017.1413196>



Published online: 14 Dec 2017.



Submit your article to this journal [↗](#)





View related articles [↗](#)



View Crossmark data [↗](#)



# High downforce race car vertical dynamics: aerodynamic index

Felipe Pereira Marchesin<sup>a</sup>, Roberto Spinola Barbosa<sup>a</sup>, Marco Gadola <sup>b</sup> and Daniel Chindamo <sup>b</sup>

<sup>a</sup>Department of Mechanical Engineering, University of Sao Paulo, Sao Paulo, Brazil; <sup>b</sup>Department of Mechanical and Industrial Engineering, University of Brescia, Brescia, Italy

## ABSTRACT

Race car performance is strongly affected by aerodynamics. Due to downforce generated by the vehicle floor (i.e. diffuser), vehicle ride heights are key parameters to improve performance, and the coupling of aerodynamics and suspension is one of the key points of race car setting. This work focuses on the suspension and aerodynamic coupling from the vertical dynamics point of view. Besides road holding performance, for race cars, aerodynamic performance and stability are major factors. Downforce decreases laptime (the main performance target) but pitch instability is a non-desired effect that can happen in high downforce race cars. A new vertical dynamic performance index is proposed through the use of simulation to improve aerodynamic performance and understand the pitch instability phenomenon. This new index uses all relevant vehicle nonlinearities related to vertical dynamics and can handle a specific track profile and vehicle speed range, allowing the analysis be conducted according to a circuit specification. A previously validated Formula 3 car model was used as an example.

## ARTICLE HISTORY

Received 14 May 2017  
Revised 18 October 2017  
Accepted 24 November 2017

## KEYWORDS

Aerodynamics; stability analysis; suspension systems

## Nomenclature

$a$	distance from sprung mass centre of gravity to front axle
AB	aerobalance
$b$	distance from sprung mass centre of gravity to rear axle
$C_m$	pitch moment coefficient
$C_{wr}$	front damping coefficient at wheel
$C_z$	downforce coefficient
$F_a$	aerodynamic force
$F_{amass}$	aerodynamic force due added mass effect
$F_{spring}$	force at suspension spring
$F_{wheel}$	spring force at wheel
gap	distance from the static position when the bump stop starts to be compressed
$h$	ride height

$K_{wr}$	spring rate at wheel
$L$	wheelbase length
$M_a$	aerodynamic pitch moment
$m_{ns}$	unsprung mass
$m_s$	sprung mass
MR	suspension motion ratio
PMI	pitch moment index
rh	ride height
$S$	vehicle frontal reference area
$t$	time
$V$	longitudinal speed
$x_{spring}$	spring displacement
$x_{wheel}$	relative displacement between wheel and sprung mass
$z_{ns}$	unsprung mass vertical displacement
$z_r$	road displacement input to the tyre
$z_s$	sprung mass vertical displacement
$\varphi_s$	sprung mass pitch angle
$\rho$	air density
$\tau$	road input time delay from front to rear axle
$\vartheta$	air volume displaced

### Subscripts

f	front
r	rear

## 1. Introduction

Nowadays the aerodynamic performance of open wheel race cars is a dominant effect over several mechanical parameters. In Formula 1, mechanical systems designs are compromised in order to improve aerodynamic performance [1]. Downforce improves braking, cornering and acceleration performance [2], from both the longitudinal and lateral dynamics point of view performance improvements can be calculated with simple quasi-static models. The influence of aerodynamics in vertical dynamics is secondary compared to the other two, but for a sport where one tenth of second can affect qualifying, this behaviour becomes important as well.

In motorsport, performance related to vertical dynamics is generated from the minimisation of the variation of tyre contact patch load from the mechanical and aerodynamic point of view. Several works have examined this [3–9], the authors worked on particular aspects concerning friction effects on race car vertical dynamics [10]. Vertical dynamics also affects driver stress conditions and performance as shown in [11].

The current state of the art approach used by the motorsport industry is the indoor test called 7 post rig [12–14], where the vehicle sprung mass is held by three actuators and there is one actuator for each tyre contact patch. The analyses of test results can be conducted in time or frequency domain. Basically, high budget series (i.e. Formula 1) use a time domain

approach as they can access enough trackside data, while medium and low budget series use the frequency domain.

There are advantages and disadvantages of both methods. Time domain simulation is done with an artificial or replicated signal of the track profile. It can use an Interactive Control System strategy, based on an interactive process that analyses the outdoor test signal and tries to replicate it creating a displacement profile in the actuators. According to some works [6] the replication process must have at least eight iterations to replicate a full race lap. To replicate a track profile, the time domain approach needs: acceleration data from the four unsprung masses, relative displacement from unsprung to sprung mass and at least one accelerometer and two gyros (pitch and roll) in the sprung mass. As shown by researchers [7] this process assures the replication of upright vertical accelerations, but it doesn't mean that the track profile is recreated. A similar method is also used by MTS [15].

Several racing series have limitations for the number of data acquisition channels as a cost control tool, and also, it is sometimes forbidden to test during events. In those cases the approach used is in the frequency domain. It is done by exciting all four wheels with a sine sweep displacement signal with decreasing amplitude with rise of frequency. Some works show improvement in performance (ranging from high downforce open wheel formulas cars to touring cars) [4,6]. These works are based on the theory that when pitch response is minimised for a bounce input it will reduce aerodynamic instability, as the longitudinal position of the centre of pressure is related to pitch attitude, resulting in a gain of mechanical grip reported by the drivers. This is based on the assumption that when the car pitches it transfer load from one axle to the other resulting a reduction of grip in one axle and an increase in the other one, changing the car balance.

Two disadvantages observed in both methods are: suspension nonlinearities are removed (e.g. bump stops) and aerodynamic coefficients are assumed constant with sprung mass movements. In time domain the aerodynamic loads are replicated from a run, but if the car settings are changed, the loads will not be the same and the replication will have errors. In frequency domain the aerodynamic forces are recreated by compressing the sprung mass over the unsprung mass through air springs (with near zero stiffness so as not to change system response) using loads calculated from steady state wind tunnel data keeping them constant through the full run. In this approach car attitude does not change the aerodynamic loads as it does on track and as can be observed from wind tunnel measurements [16]. The test is sometimes also conducted together with simulations in order to reduce the number of runs [14].

Race car configurations (i.e. aerodynamic and suspension settings) change according to race track characteristics. The track layout will determine the speed range the race car will operate in. Table 1 shows the characteristics of different tracks, the aerodynamic configuration used, bump level (qualitative information about unevenness of the road excluding the curbs), and speed range. Even with the same aerodynamic configuration, the speed range changes.

This work presents a method of calculating an aerodynamic performance index related to vertical dynamics transient response using simulation. This index is calculated in frequency domain and represents the aerodynamic pitch moment statistical variance over a speed range for a specific vehicle configuration (i.e. wings setting, springs and bump stops). Tyre grip is a function of vertical load and friction coefficient. The more steady the aerodynamic loads are, the less variation the wheel loads will have and the better will be the

**Table 1.** Track characteristics differences from five different circuits.

Circuit	Aerodynamic configuration	Bump level	Speed (km/h)	
			min	max
circuit 1	High downforce	high	56	216
circuit 2	High downforce	low	80	224
circuit 3	High downforce	low	66	238
circuit 4	Medium downforce	medium	62	245

overall vehicle performance. This new method will include both aerodynamic and suspension nonlinearities in the car model, and will be simulated at different longitudinal speed ranges, characterising the vertical dynamics behaviour as a function of speed.

### 2. Proposed model

The half car model is a classic model used to evaluate vertical dynamics. In its complete form it has four degrees of freedom; pitch and bounce (angular and vertical movements of mass centre) for sprung mass, and front and rear unsprung mass vertical displacements. The model described below is an upgrade from the classic half car model, it incorporates a nonlinear suspension and an aerodynamic model. The suspension damping and tyre stiffness are linear. Figure 1 shows the model degrees of freedom and the reference system.

The aerodynamic model is divided into downforce and pitch moment, the pole being where the front axle crosses the ground. Equations (1)–(4) represent: pitch, bounce, front unsprung and rear unsprung equations of motion respectively.

$$I_y \ddot{\alpha}_{ns} = M_a + a F_a + F_{wheel f} a + F_{wheel r} b + c_{wf} (-\dot{z}_s + \dot{\varphi}_s a + \dot{z}_{nsf}) a + c_{wr} (\dot{z}_{nsr} - \dot{z}_s - \dot{\varphi}_s b) b, \tag{1}$$

$$m_s \ddot{z}_s = -F_a + F_{wheel f} + F_{wheel r} + c_{wf} (\dot{z}_s - \dot{\varphi}_s a - \dot{z}_{nsf}) + c_{wr} (\dot{z}_{nsr} - \dot{z}_s - \dot{\varphi}_s b), \tag{2}$$

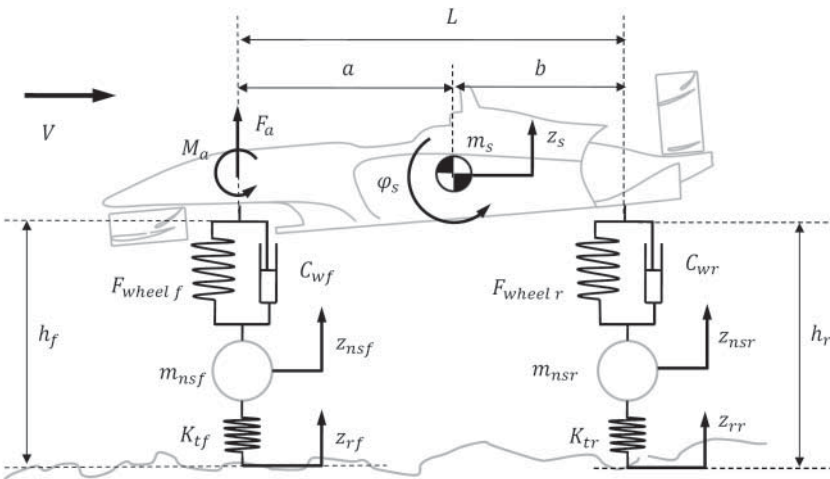


**Figure 1.** Half car model.

$$m_{\text{nsf}}\ddot{z}_{\text{nsf}} = +F_{\text{wheelrf}} + c_{\text{wf}}(\dot{z}_{\text{s}} - \dot{\phi}_{\text{s}}a - \dot{z}_{\text{nsf}}) + k_{\text{tf}}(z_{\text{rf}} - z_{\text{nsf}}), \quad (3)$$

$$m_{\text{nsr}}\ddot{z}_{\text{nsr}} = F_{\text{wheelrf}} + c_{\text{wr}}(\dot{z}_{\text{nsr}} - \dot{z}_{\text{s}} - \dot{\phi}_{\text{s}}b) + k_{\text{tr}}(z_{\text{rr}} - z_{\text{nsr}}). \quad (4)$$

The spring forces were modelled as nonlinear forces with spring displacements. The Equations (5) and (6) present the time delay between front and rear axle inputs due to surface roughness.

$$z_{\text{rr}}(t) = z_{\text{rf}}(t - \tau), \quad (5)$$

$$\tau = \frac{L}{V}. \quad (6)$$

The aerodynamic forces and the spring stiffness are treated as nonlinear functions. The first is nonlinear mainly because of the ground effect, downforce increases when an aerofoil/diffuser is closer to the ground due mainly to the interruption of the tip vortices [2]. The second, because of the need to resist high aerodynamic loads, the suspension has a nonlinear stiffness device in parallel to the spring to progressively increase the total system stiffness (e.g. bump stop). As the vehicle speed increases, downforce increases, the suspension is compressed and ride height is lower. Lower ride heights increase the downforce coefficient because of the ground effect.

## 2.1. Aerodynamic forces

The aerodynamic force and pitch moment are calculated using Equations (7) and (8).

$$F_{\text{a}} = \frac{1}{2}\rho SC_z V^2 = pSC_z, \quad (7)$$

$$M_{\text{a}} = \frac{1}{2}\rho SC_m LV^2 = pLSC_m. \quad (8)$$

The nonlinear aerodynamic coefficients presented in Equations (9)–(11) are based on methods used by other authors [16] and by the industry [15].

$$C_z = C_{z0} + \frac{\partial C_z}{\partial h_f} h_f + \frac{\partial C_z}{\partial h_r} h_r + \frac{\partial^2 C_z}{\partial h_f^2} h_f^2 + \frac{\partial^2 C_z}{\partial h_r^2} h_r^2 + \frac{\partial^2 C_z}{\partial h_f \partial h_r} h_f h_r, \quad (9)$$

$$C_m = C_{m0} + \frac{\partial C_m}{\partial h_f} h_f + \frac{\partial C_m}{\partial h_r} h_r + \frac{\partial^2 C_m}{\partial h_f^2} h_f^2 + \frac{\partial^2 C_m}{\partial h_r^2} h_r^2 + \frac{\partial^2 C_m}{\partial h_f \partial h_r} h_f h_r, \quad (10)$$

$$AB = AB_0 + \frac{\partial AB}{\partial h_f} h_f + \frac{\partial AB}{\partial h_r} h_r + \frac{\partial^2 AB}{\partial h_f^2} h_f^2 + \frac{\partial^2 AB}{\partial h_r^2} h_r^2 + \frac{\partial^2 AB}{\partial h_f \partial h_r} h_f h_r = \left(1 + \frac{C_m}{C_z}\right). \quad (11)$$

The vehicle used as example presents a maximum error of 3% between the regression and the experimental data, Figure 2 presents a comparison between the proposed model (dashed lines) and wind tunnel measurements (solid lines). Both downforce coefficient (left plot) and aerobalance (right plot) present less than a 1% error and the pitch moment coefficient (middle plot) presents a higher error mainly due to diffuser stall (rear ride height lower than 20 mm) while in the in the other regions the model represents the coefficient accurately.

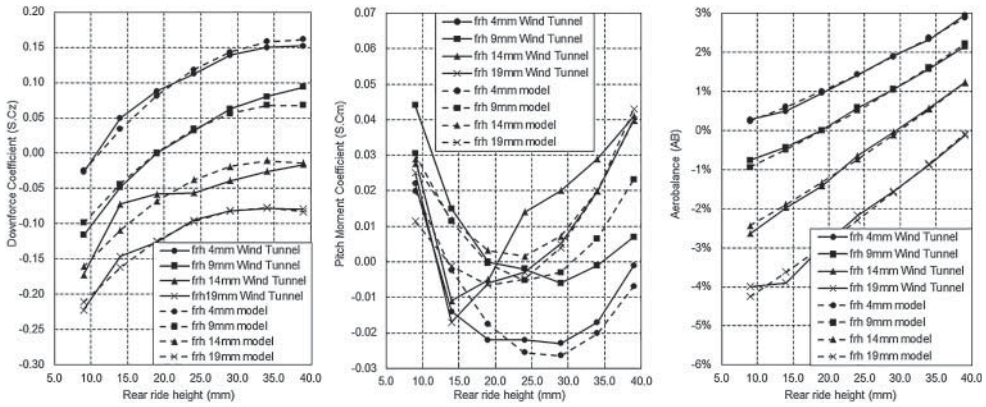


**Figure 2.** Comparison between the regression model and wind tunnel measurements for downforce coefficient, pitch moment coefficient and aerobalance at different front and rear ride heights. The plots show relative values as data is classified.

In general, the pitch moment coefficient is not used by the motorsport industry. The race car manufacturers supply a parameter called aerobalance [16,17–20], it represents the percentage of the total downforce acting on the vehicle front axle. It is very useful for quasi-static analysis as it is compared to the vehicle static weight distribution in order to have an idea of how much understeer/oversteer tendency (i.e. car balance) is expected at high speeds. For the purpose of this work it is not the main parameter to be analysed. Aerobalance is not directly a function of speed, it changes because of sprung mass movements. The pitch moment is the pitch moment coefficient multiplied by the dynamic pressure, which makes the moment increase with the square of speed. Also the pitch moment coefficient is a combination of both downforce coefficient and aerobalance, as showed in Equation (11). This means that it combines the variation of both. As an example, increases of aerobalance with decrease of downforce do not change aerodynamic pitch moment and aren't important from the pitch performance/stability point of view. The pitch moment coefficient is also used by the aerospace industry to analyse flight dynamics [21].

The aerodynamic coefficients from wind tunnel measurements, normally use front and rear ride heights as variables. In order to relate pitch moment to pitch displacement, the front ride height will be kept as a variable, Equation (12), and rear ride height will be substituted by pitch angle, according to Equation (13). This new aerodynamic reference coordinate system also has been chosen for the front axle in order to make it possible to compare different cars, as the centre of mass position changes from car to car.

$$z = h_f, \quad (12)$$

$$\varphi = \frac{h_r - h_f}{L}. \quad (13)$$

The equations for the aerodynamic coefficients in the new reference system are presented in Equations (14) and (15) and will be used in quasi-static calculations.

$$C_z = C_{z0} + \frac{\partial C_z}{\partial z} z + \frac{\partial C_z}{\partial \varphi} \varphi + \frac{\partial^2 C_z}{\partial z^2} z^2 + \frac{\partial^2 C_z}{\partial \varphi^2} \varphi^2 + \frac{\partial^2 C_z}{\partial z \partial \varphi} z \varphi. \quad (14)$$



$$C_m = C_{m0} + \frac{\partial C_m}{\partial z} z + \frac{\partial C_m}{\partial \varphi} \varphi + \frac{\partial^2 C_m}{\partial z^2} z^2 + \frac{\partial^2 C_m}{\partial \varphi^2} \varphi^2 + \frac{\partial^2 C_m}{\partial z \partial \varphi} z \varphi. \quad (15)$$

In transient behaviour the aerodynamic coefficients are linearised for each value of longitudinal speed. Using this approach, equations were formulated, for both downforce and moment, as presented in Equations (16)–(18).

$$C_{z(v)} = C_{z\text{base}} + \frac{\partial C_z}{\partial \varphi} \varphi + \frac{\partial C_z}{\partial z} z, \quad (16)$$

$$\frac{\partial C_z}{\partial \varphi} = \frac{\partial C_z}{\partial \varphi} + 2 \frac{\partial^2 C_z}{\partial \varphi^2} \varphi + \frac{\partial^2 C_z}{\partial z \partial \varphi} z, \quad (17)$$

$$\frac{\partial C_z}{\partial z} = \frac{\partial C_z}{\partial z} + 2 \frac{\partial^2 C_z}{\partial z^2} z + \frac{\partial^2 C_z}{\partial z \partial \varphi} \varphi. \quad (18)$$

In order to input the transient aerodynamic forces, the approach used follows works published concerning unsteady aerodynamics in ground effect [22]. They show that three main effects are important for unsteady aerodynamics: the ground clearance, the induced angle of attack and the added mass. They are proportional to vertical displacement (stiffness), speed (damping) and acceleration (inertia) respectively. Each one of them has its main effect in a specific range of frequency response.

In the present model the effect of added mass (inertia effect) will be neglected as it affects high frequencies and the main effects of interest are below 60 Hz. The excitation frequency range (0.1–60 Hz) chosen includes the sprung mass and the unsprung mass natural frequencies over all the speed range as presented in Figure 7 (from 3.5 Hz up to 47 Hz). The added mass effect for a bounce displacement can be estimated by Equation (19) [22]. The vehicle floor area [19] and displacement amplitude were estimated as 3.5 m<sup>2</sup> and 10 mm.

$$F_{\text{amass}}(t) = \rho \vartheta \frac{d^2 z}{dt^2}. \quad (19)$$

From Equation (19), the maximum downforce induced by the added mass effect can be estimated as presented in Equation (20).

$$\bar{F}_{\text{amassmax}} = \rho \vartheta z_{\text{max}} (2\pi f)^2. \quad (20)$$

Using Equation (20) and the estimated data, the maximum downforce would be around 60 N at 60 Hz. As it is low compared to other effects it can be neglected.

However, aerodynamic damping and stiffness affects low and medium range frequencies. The stiffness was already computed in Equations (14) and (15) as they are functions of the sprung mass displacement (pitch and bounce). The damping, on the other hand, must be added. If the air flow keeps attached to the aerodynamic surface the angle of attack can be substituted by the induced angle of attack [20]. In this way, the pitch angle will be a function of pitch displacement, pitch speed and bounce speed, as presented in



Equation (21).

$$\varphi = \varphi_s + \dot{\varphi}_s \frac{L}{V} + \frac{\dot{z}_s}{V}. \quad (21)$$

To convert the aerodynamic coefficients coordinates system into the equations of motion coordinate system (origin at centre of gravity), the front axle displacement must be rearranged to be a function of centre of mass, and sprung mass pitch displacement according to Equation (22).

$$z = z_s + \varphi_s a. \quad (22)$$

Using both the induced angle of attack presented in Equation (21), and the new reference for vertical displacement presented in Equation (22) into Equation (16) for both coefficients, they can be calculated as presented in Equations (23) and (24). These equations calculate the downforce and pitch moment coefficient using pitch and bounce displacement and also their first derivative over time. This approach includes aerodynamic stiffness and damping in the model. They are used in the transient model, and their terms are included in the equations of motion in state space format presented in Equation (34).

$$\begin{aligned} C_{z(v)} = C_{z(v)} + \left( \frac{\partial C_z}{\partial z} \frac{1}{(v)} a + \frac{\partial C_z}{\partial \varphi} \frac{1}{(v)} \right) \varphi_s + \left( \frac{\partial C_z}{\partial \varphi} \frac{L}{(v) V} \right) \dot{\varphi}_s \\ + \left( \frac{\partial C_z}{\partial z} \frac{1}{(v)} \right) z_s + \left( \frac{\partial C_z}{\partial \varphi} \frac{1}{(v) V} \right) \dot{z}_s, \end{aligned} \quad (23)$$

$$\begin{aligned} C_{m(v)} = C_{m(v)} + \left( \frac{\partial C_m}{\partial z} \frac{1}{(v)} a + \frac{\partial C_m}{\partial \varphi} \frac{1}{(v)} \right) \varphi_s + \left( \frac{\partial C_m}{\partial \varphi} \frac{L}{(v) V} \right) \dot{\varphi}_s \\ + \left( \frac{\partial C_m}{\partial z} \frac{1}{(v)} \right) z_s + \left( \frac{\partial C_m}{\partial \varphi} \frac{1}{(v) V} \right) \dot{z}_s. \end{aligned} \quad (24)$$

## 2.2. Spring model

Race cars must adjust the suspension system to maximise performance on track. This implies that the car ground clearance must be as low as possible. Due to aerodynamics, as speed increases, the suspension is subjected to higher loads and ground clearance decreases. At first glance, the key point is to set the race car to avoid touching the ground and because of that the suspension stiffness must be high. Nonlinear springs are not as common on race cars as on road cars, and normally a bump stop is used to help the spring to set the proper ground clearance against speed.

In order to include the effects of the bump stop, a nonlinear spring stiffness curve was used. Figure 3 shows the relationship between force and displacement for a bump stop from measurement data. This force was modelled using a fourth-order polynomial regression and used in the quasi-static calculations.

The bump stop is not always being compressed, a gap measured at the static position between the bump stop and the damper body is used to set its starting position. Equation (25) presents how the model was implemented.

$$\text{If } x_{\text{spring}} < \text{gap},$$

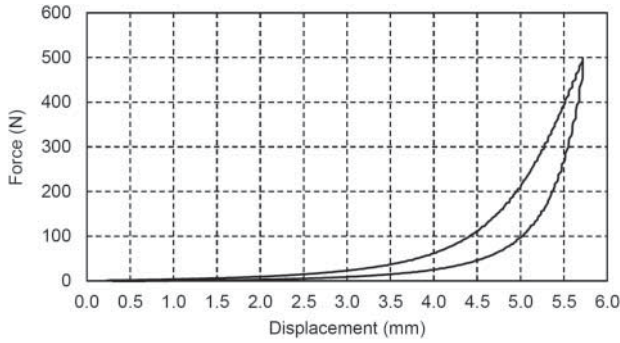


**Figure 3.** Bump stop force and displacement curve.

$$F_{\text{spring}} = Kx_{\text{spring}},$$

Else,

$$F_{\text{spring}} = Kx_{\text{spring}} + a_1(x_{\text{spring}} - \text{gap}) + a_2(x_{\text{spring}} - \text{gap})^2 + a_3(x_{\text{spring}} - \text{gap})^3 + a_4(x_{\text{spring}} - \text{gap})^4. \quad (25)$$

The hysteresis effects of the bump stop were not included in the model as they are another nonlinear effect and their magnitude is small if compared to the damper characteristics (some suspension configurations can use high hysteresis bump stops [23], but they aren't used in the current work). The authors previous work in race car suspension hysteresis influence on vertical dynamics show its undesirable effects [10].

The spring force is calculated using a linear motion ratio, Equation (26). The spring's displacement uses the same approach, as presented in Equations (27) and (28) for front and rear axle, respectively.

$$F_{\text{wheel}} = \frac{F_{\text{spring}}}{\text{MR}}, \quad (26)$$

$$x_{\text{wheel f}} = x_{\text{spring f}} \text{MR} = (-z_s + \varphi_s a + z_{\text{nsf}}) \text{MR}, \quad (27)$$

$$x_{\text{wheel r}} = x_{\text{spring r}} \text{MR} = (z_{\text{nsr}} - z_s - \varphi_s b) \text{MR}. \quad (28)$$

In the transient calculations, the stiffness is linearised for each value of longitudinal speed (trim position).

### 3. Results

The following results are divided into quasi-static and transient. The quasi-static results are used to show why some nonlinearities must be included in a high downforce racecar vertical dynamics model in order to achieve meaningful results and also, to calculate the trim positions to be used in the transient model. The transient results present the frequency responses that will be used to calculate the proposed index.

Simulations are based on a Formula 3 car used in competition from 2012 up to 2016. All data used to supply the model comes from measurements (courtesy of Fortec Motorsports), the model has been validated for work application purposes (quasi-static ride

height prediction, lap time simulation and driver simulator) and also used in a previous work [24].

### 3.1. Quasi-static

One of the key indicators in quasi-static vertical dynamics is the dynamic ride height, it is the axle ride height as function of the speed. The race car model presented in Equations (1)–(4) is subjected to a longitudinal speed sweep (from 0 km/h up to 230 km/h), neglecting longitudinal and lateral acceleration. This is a common procedure to calculate quasi-static ride heights [25]. Figure 4 shows the race car ride heights, pitch angle and tyre deflection in this condition.

In the far left graph of Figure 4, it is possible to see that the rear ride height changes its trend (due a change in suspension stiffness) while the front doesn't. This occurs because the front suspension at static position already touches the bump stop (zero gap), while the rear suspension has a gap of 6 mm to touch the bump stop. The left hand graph in Figure 4 also shows the bump stop entry at 100 km/h, at around 24 mm rear ride height (12 mm of ride height displacement), and the right hand graph shows that at 100 km/h the rear tyres are compressed by around 3.5 mm, meaning a suspension displacement of 8.5 mm at this speed. As the bump stop needs some compression in order to build up a force that can change the suspension behaviour, the 6 mm gap in the rear suspension starts to affect the system around 100 km/h.

Another particularity from race cars are the tyres; they generally are of high profile and are designed mainly to maximise grip. Because of that, the vertical stiffness is generally less than a road tyre. This, in combination with a high stiffness suspension, can achieve a stiffness ratio around 1:1. At high speed the suspension can have its stiffness increased by the bump stop, which can lead suspension vertical stiffness to be much higher than tyre

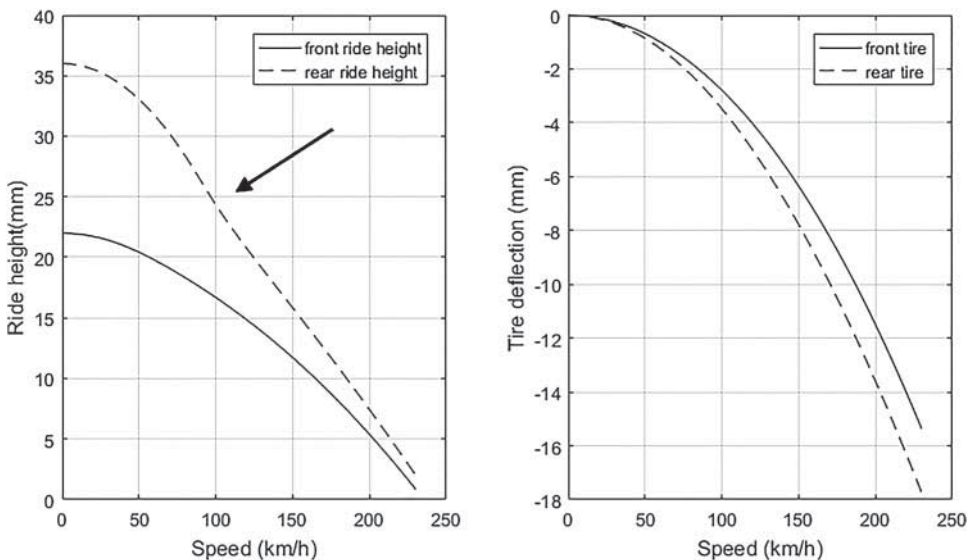


**Figure 4.** Dynamic ride heights pitch displacement and tyre deflection.

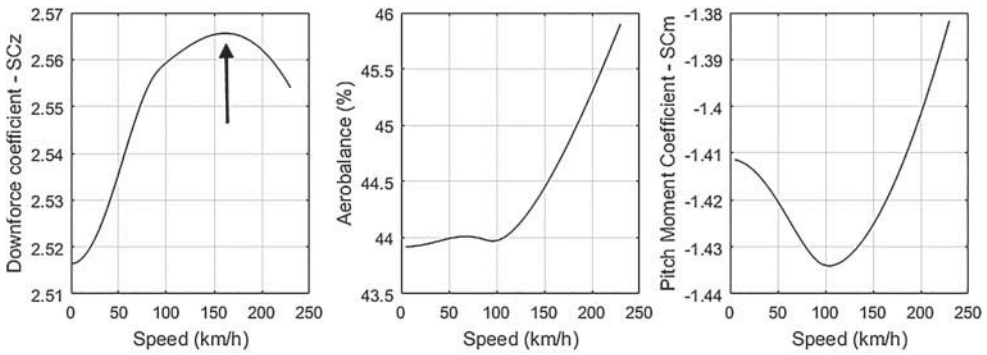


**Figure 5.** Aerodynamic parameters as function of speed.

stiffness. If tyre stiffness is less than suspension stiffness it becomes a dominant factor in the dynamic behaviour, and the spring and damper start to have less contribution to the system response, leaving the system almost undamped. In Figure 4, of 22 mm total displacement of the front axle, 15 mm is tyre deflection, and of 36 mm at the rear axle, 18 mm belongs to tyre deflection.

At a second glance, but no less important, the dynamic ride heights affect the aerodynamic performance. Because the car ground clearance is very low, it benefits from ground effect in generating more downforce. As the aerodynamic coefficients are a function of front and rear ride heights, setting the correct dynamic ride heights for each track can optimise overall performance. Figure 5 shows the downforce coefficient, aerobalance and pitch moment coefficient for the longitudinal speed sweep (from 0 km/h up to 230 km/h).

The inflection point in the downforce coefficient at 150 km/h presented in the left plot of Figure 5 is a typical diffuser stall, which happens when the rear ride height becomes too low. This drop of downforce also results a drop in drag, desirable at high speeds to increase straight line speed. As the pitch moment coefficient is a function of both downforce coefficient and aerobalance, it shows a sharper inflection point than aerobalance.

### 3.2. Transient

Race car vertical dynamics is a compromise between aerodynamic stability and road holding. The first one is affected by the pitch moment and the second is affected by the tyre contact patch load variation. When speed increases, the race car ground clearance and the suspension stiffness change, and because of these effects, vehicle frequency response changes as well.

The equations of motion presented before, Equations (1)–(4), have their suspension stiffness and aerodynamic coefficients linearised for a range of speed values (from 0 km/h up to 230 km/h) and transformed into a first-order state space differential system of equations as presented in Equation (29). Pitch and bounce displacement, aerobalance and pitch moment are calculated as outputs as shown in Equation (30). Aerodynamic pitch moment was chosen as an output instead of the pitch moment coefficient, as it increases with speed. A small variation of the coefficient at high speed is magnified due to the speed value. Matrix **A** is not diagonal, resulting in coupled modes. This means that the vehicle doesn't behave

in pitch and bounce movements in an uncoupled way. The coupled modes are nominated: front-end bounce and rear-end bounce [26]. Additionally, the rear tyre input was modelled with a time delay – last item of Equation (29) – a function of speed and wheelbase length, as formulated in Equation (6).

$$\begin{bmatrix} \dot{z}_s \\ \dot{\alpha}_s \\ \dot{z}_{nsf} \\ \dot{z}_{nsr} \\ \dot{\omega}_s \\ \dot{v}_s \\ \dot{v}_{nsf} \\ \dot{v}_{nsr} \end{bmatrix} = A \cdot \begin{bmatrix} z_s \\ \alpha_s \\ z_{nsf} \\ z_{nsr} \\ v_s \\ \omega_s \\ v_{nsf} \\ v_{nsr} \end{bmatrix} + \begin{bmatrix} 0 \\ 0 \\ 0 \\ 0 \\ 0 \\ 0 \\ 1 \\ 0 \end{bmatrix} u(t) + \begin{bmatrix} 0 \\ 0 \\ 0 \\ 0 \\ 0 \\ 0 \\ 0 \\ 1 \end{bmatrix} u(t - \tau), \quad (29)$$

$$\begin{bmatrix} z \\ \varphi \\ AB \\ M \end{bmatrix} = \begin{bmatrix} 1 & 0 & 0 & 0 & 0 & 0 & 0 & 0 \\ 0 & 1 & 0 & 0 & 0 & 0 & 0 & 0 \\ \frac{\partial AB}{\partial z} & \frac{\partial AB}{\partial h} a + \frac{\partial AB}{\partial \varphi} & 0 & 0 & \frac{\partial AB}{\partial \varphi} \frac{1}{V} & \frac{\partial AB}{\partial \varphi} \frac{L}{V} & 0 & 0 \\ pLS \frac{\partial C_m}{\partial z} & pLS \left( \frac{\partial C_m}{\partial z} a + \frac{\partial C_m}{\partial \varphi} \right) & 0 & 0 & pLS \frac{\partial C_m}{\partial \varphi} \frac{1}{V} & pLS \frac{\partial C_m}{\partial \varphi} \frac{L}{V} & 0 & 0 \end{bmatrix} \times \begin{bmatrix} z_s \\ \alpha_s \\ z_{nsf} \\ z_{nsr} \\ v_s \\ \omega_s \\ v_{nsf} \\ v_{nsr} \end{bmatrix} + \begin{bmatrix} 0 \\ 0 \\ 0 \\ 0 \end{bmatrix} u(t). \quad (30)$$

Using the equations derived above, the transfer functions were obtained and shown in Figures 6. The effect of wheelbase filtering [27] in the frequency response is shown by the peaks and valleys presented in the front-end and rear-end bounce modes plotted at the left side of Figure 6. The peaks and valleys mean a specific input frequency that, because of the time delay between front and rear inputs, will maximise one mode response while almost not affecting by the other mode. As the vehicle goes faster, the difference in frequency values between the two consecutive peaks and two consecutive valleys becomes smaller. This effect is not included when the vehicle is subjected to a bounce sine sweep input as used in the 7 post rig test, representing one more improvement from the present approach.

The left plots of Figure 6 show the two modes of the sprung mass (front and rear end bounce). Besides the effects of wheelbase filtering, they show that the modes change their natural frequency and damping as speed increases. This is expected as the suspension stiffness increases, due to bump stop nonlinearity, and also the aerodynamic forces change stiffness and damping in the system. A quantitative analysis from these plots was made in Figure 7, showing the system natural frequencies and damping as function of speed. The right side plots of Figure 6 shows aerobalance and aerodynamic pitch moment frequency response. A comparison between them shows that at high speeds the aerodynamic pitch

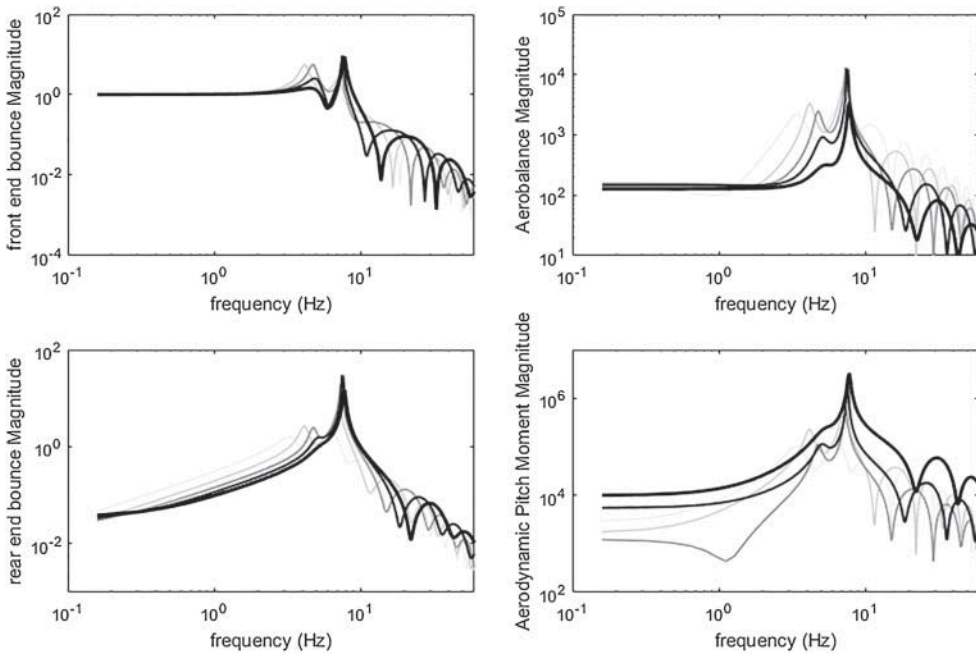


**Figure 6.** System sprung modes displacement, aerobalance and aerodynamic pitch moment frequency response (speed range from 70 km/h up to 230 km/h, being higher speeds in darker colours).

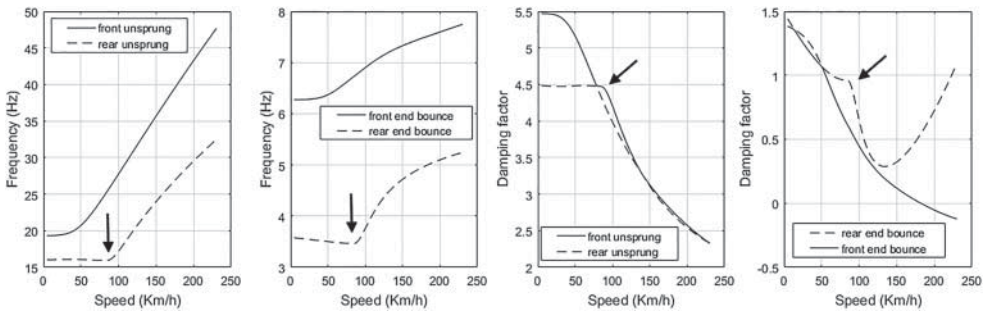


**Figure 7.** System natural frequencies and damping ratio.

moment gain increases while the aerobalance decreases. This happens mainly because aerodynamic pitch moment increases with the square of speed, while the aerobalance changes according to vehicle attitude.

Figure 7 presents the natural frequencies and the damping ratios. The rear bump stop starts to increase rear suspension stiffness around 100 km/h, as also shown in Figure 4. The consequences in both natural frequency and damping are shown in Figure 7 by the black arrows. Rear-end bounce natural frequency starts to increase after the bump stop engages in the suspension system, while the front-end bounce is always increasing as the bump stop is being compressed from static position onwards. A similar behaviour is shown in the damping, the increase of bump stop stiffness decreases the damping. In the rear-end



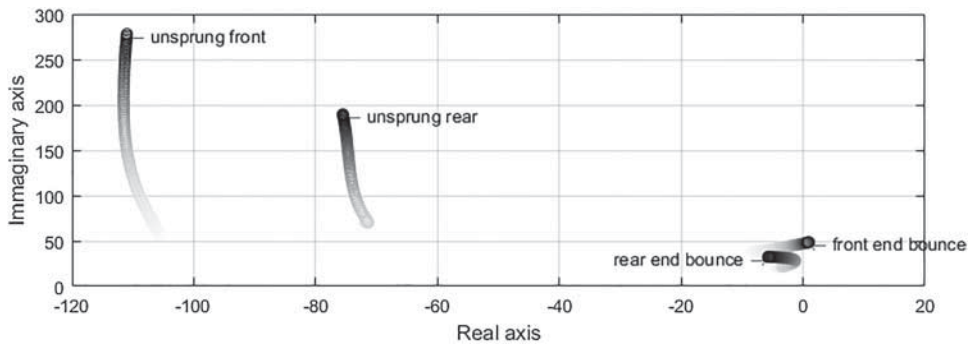


**Figure 8.** System Eigen values as function of speed (darker values represent high speeds, from 0 km/h up to 230 km/h).

bounce mode, before the bump stop is engaged, the damping is constant, and after it starts working damping decreases. In the front-end bounce mode the damping is always decreasing as the front gap is 0 mm. The diffuser stall can also be observed: between 100 and 150 km/h rear-end bounce damping changes its trends. Before the stall the damping decreases and after it the damping starts to increase again. The right plot from Figure 7 shows the front-end bounce has negative values of damping at high speeds. These negative values mean that the mode is unstable in this speed range, any input from the road will lead to vertical vibrations that keep increasing.

There is also one more important effect to analyse, the pitch instability. Figure 8, presents the system roots as a function of speed (darker values represent high speeds, the range is from 0 km/h up to 230 km/h), and shows that the front-end bounce migrates to instability (positive values in the real axis). Changes in car settings (e.g. suspension stiffness, damping and ride height) can make the system stable. The standard approach is less stiffness (softer bump stop or bigger gap) and more damping (adjustable by changes to the damper). An extrapolation from the results present in Figure 7 show that bigger gaps and softer bump stops would shift system natural frequencies and the damping inflection point (black arrow). Another way is the use of high hysteresis bump stops [24].

Although the rear axle has a loss of downforce because of the diffuser stall, it is on the front axle that aerodynamics is critical. Damping ratios are very high at low speed, but they become lower at higher speeds. The closer to the ground the front axle is, the higher the front suspension stiffness becomes (needing more damping), and the aerodynamics become more sensitive, resulting in a decrease of front-end modal damping (negative values over 180 km/h) and leading to instability.

#### 4. Proposed performance index

The proposed performance index (pitch moment index – PMI) calculates how much pitch moment variability a specific vehicle configuration has in a specific speed range. In order to create this, the aerodynamic pitch moment transfer function for a full operation speed range (in the example from 0 km/h up to 235 km/h, in steps of 2.5 km/h) is used together with an artificial road profile (asphalt roughness type ‘C’ – ISO standard) to calculate the pitch moment gain for each speed step (Figure 10). The integration of each pitch



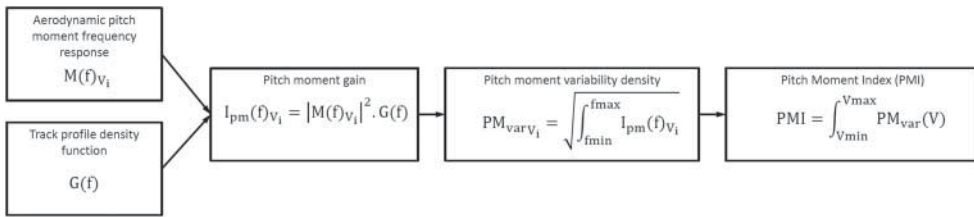


Figure 9. Index calculation flow chart.

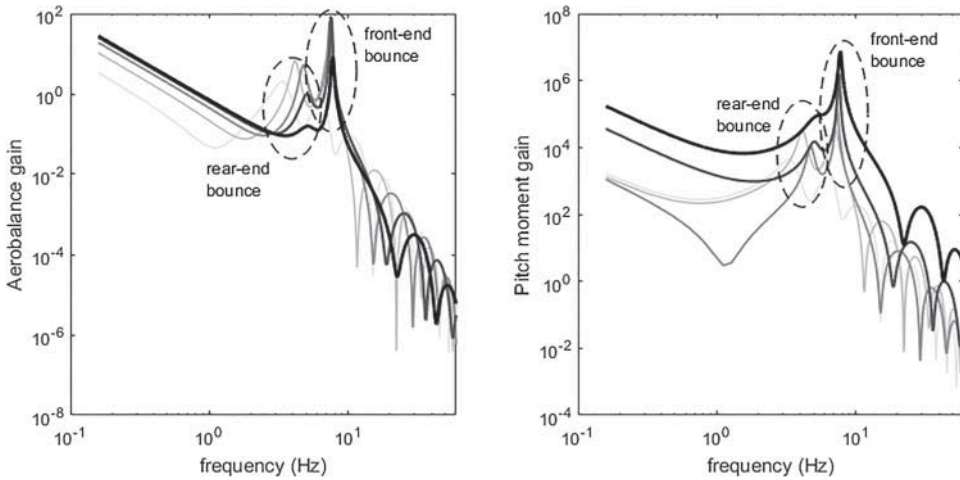
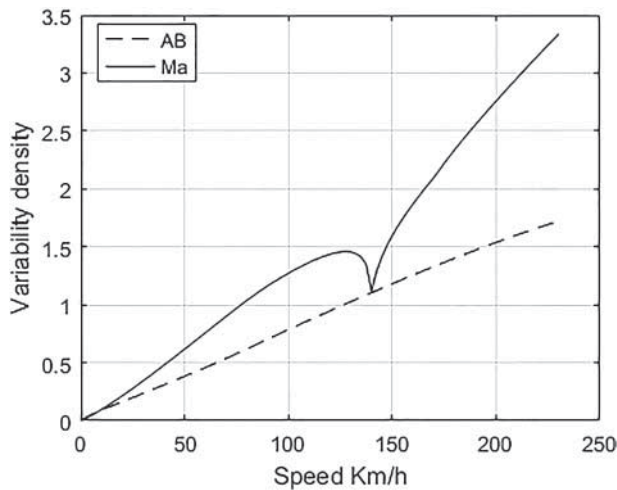


Figure 10. Aerobalance and pitch moment gain functions as functions of speed (dark values represent higher speeds).

moment gain curve over the frequency range gives a pitch moment variability density (also described as statistical variance) as a function of speed (Figure 11). The PMI is calculated integrating the pitch moment variability density over the speed range. Figure 9 explains the performance index calculation process. For comparison purposes, the same procedure was conducted with aerobalance frequency response.

Figure 10 presents the aerobalance and pitch moment gain as a function of frequency for the artificial road used. Aerobalance increases its gain with speed at frequencies under 1 Hz and at 7 Hz (close to front-end bounce natural frequency), for all other frequency ranges it decreases. After 7 Hz, the gain decreases more sharply up to 60 Hz. On the other hand, pitch moment has a small decrease in frequencies under 4 Hz at medium speeds (diffuser stall), but overall higher gains at higher speeds. After 10 Hz, the gain starts to decrease. The higher gain of pitch moment at higher speeds is caused by its increase with the square of the speed. Both plots have a similar shape as pitch moment is a function of aerobalance and downforce – Equation (11). They will present peaks at the system natural frequencies: front-end bounce (between 3.5 and 5.5 Hz) and rear-end bounce (between 6.3 and 7.5 Hz), as shown in Figure 7.

Figure 11 shows the pitch moment and aerobalance variability density as a function of speed, for a speed range from 0 km/h up to 235 km/h. The sudden decrease around



**Figure 11.** Pitch moment and aerobalance variability density.

150 km/h in the pitch moment is caused by the diffuser stall, while the aerobalance does not show any influence of the diffuser stall. This is one of the main reasons that pitch moment was chosen over aerobalance to represent system response to aerodynamic effects.

In order to check the influence of vehicle configuration in the proposed index, a value sweep of some parameters was conducted and presented in Figure 12. A baseline configuration (low ride heights with stiff suspension configuration) is also present in all plots for comparison purposes. The left hand graphs show a ride height sweep (front ride height on top and rear on the bottom), the middle graphs show a gap sweep (front gap on top and rear on the bottom), and the right hand graphs show on top a comparison moving the centre of pressure forward and backwards ( $C_m$  minus 2% and  $C_m$  plus 2%) and on the bottom the comparison of the baseline with a configuration where the suspension is soft and tyre stiffer. From all the configurations tested the only one, which avoids the diffuser stall is when the rear ride height is over 37 mm (bottom left graph of Figure 12). All other configurations, even those not avoiding the diffuser stall, affect the pitch moment variability density, showing that the proposed index (PMI) is sensitive to vehicle configuration changes, as it is a function of pitch moment variability density (Figure 9).

Figure 13 shows the aerodynamic parameters (downforce coefficient, pitch moment coefficient and aerobalance) for the configurations in the first and second columns presented in Figure 12 (ride heights and gaps). The diffuser stall is also noticed in the coefficients plots (inflection of downforce coefficient curve, plots in the top row of Figure 13). It also shows that aerobalance has no inflection point (plots of the third row of Figure 13) in comparison to the pitch moment coefficient (plots in the second row of Figure 13) when the diffuser stalls. Pitch moment coefficient was used to calculate pitch moment, Equation (8), which increases with the square of speed, magnifying the effect of speed and also the small variations of the pitch coefficient at high speeds. Figure 13 also shows that the pitch moment coefficient changes over the full speed range with rear ride height sweep whilst the others parameters affects mainly low speed. As the speed value after the inflection point

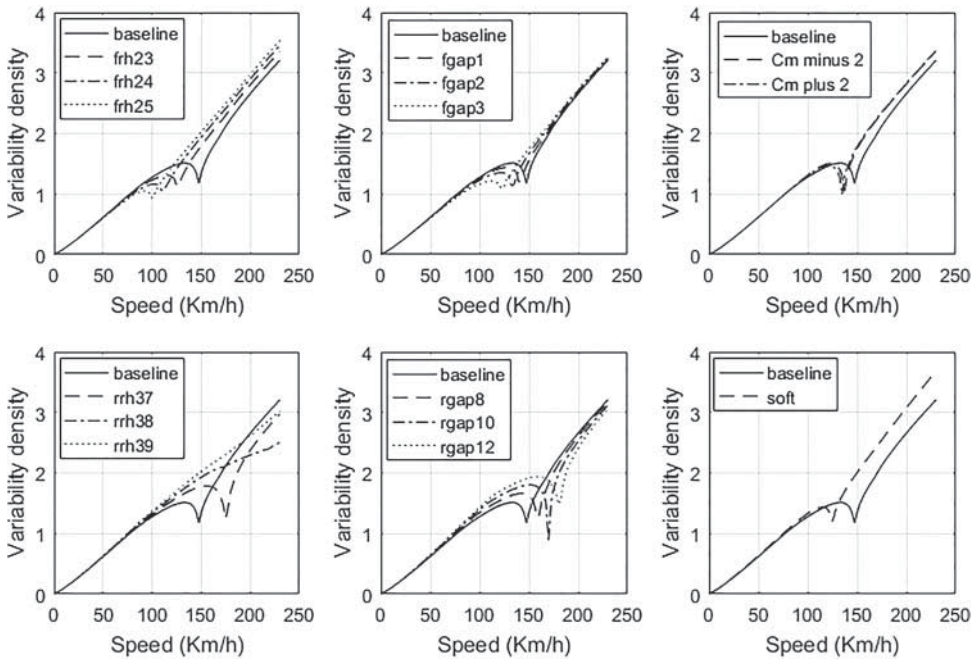


Figure 12. Pitch moment variability density sensibility check.

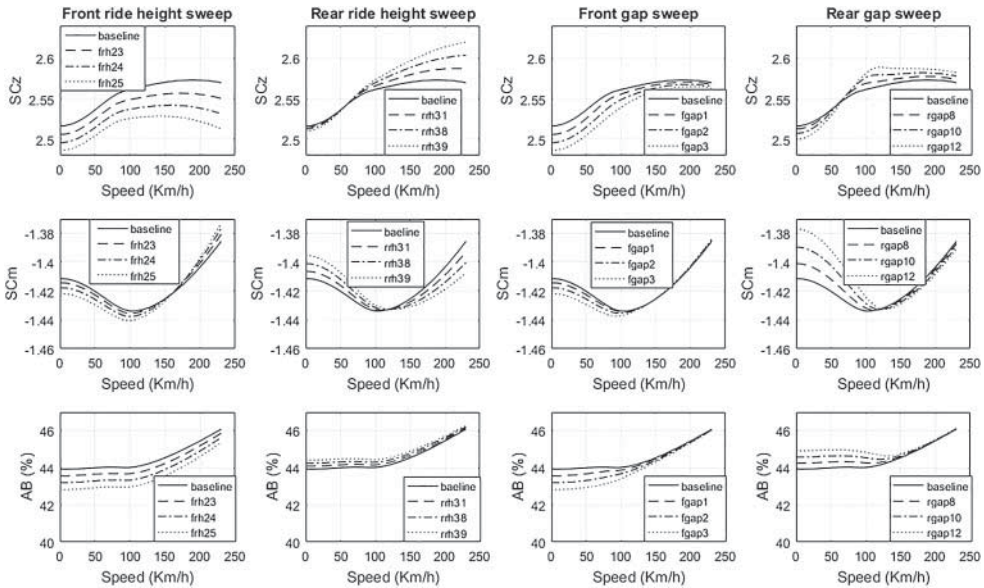
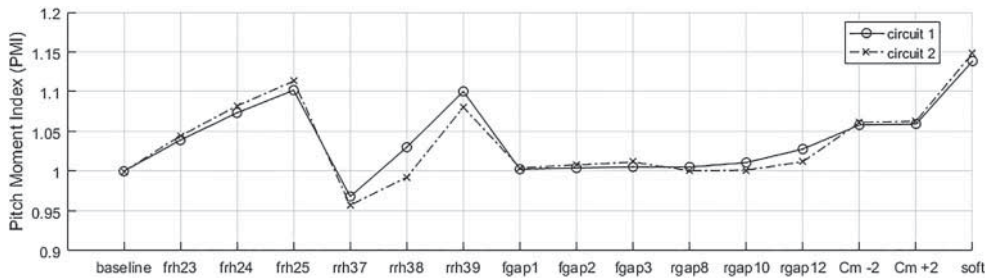


Figure 13. Aerodynamic coefficients for the configurations used in the sensibility check.

is high, the Pitch Moment will be magnified by it, increasing the influence of the configuration change even at high speeds. These observations show that pitch moment is a better choice as performance index than the pitch moment coefficient and is also better than aerobalance.



**Figure 14.** PMI comparison.

Integrating the curves from Figure 12, the PMI was calculated and shows how much statistical variance from the aerodynamic pitch moment is expected for each configuration in comparison to the baseline (the values were normalised by the baseline) and this is presented in Figure 14. The integration was conducted for the speed ranges from circuit 1 and circuit 2 presented in Table 1.

Besides the differences in the pitch moment variability density showed in Figure 12, the PMI shows, as expected, different values according to different target speed ranges. One of the most important aspects is that some configurations show different trends. For both circuits analysed, the increase of front ride height increases the index, but for a rear ride height of 38 mm, for example, the index is smaller than the baseline in circuit 1 and higher in circuit 2. The differences will be bigger when comparing circuits with a big difference in speed ranges and in aerodynamic packages as well.

Figure 14 also shows that an increase of both front and rear ride heights lead to an increase of PMI, while aerobalance (third row of Figure 13) will decrease with a higher front ride height (meaning understeer) and will increase with rear ride height (meaning oversteer).

## 5. Conclusions

In this work a novel vehicle performance index related to design and setup parameters has been presented. This index evaluates the pitch moment statistical variance over a specific speed range defined by each specific race track.

A 4-DoF model with nonlinear suspension and aerodynamic forces has been used to evaluate the index effectiveness and reliability. This model has been validated in a previous work and it also includes transient effects such as the influence of angle of attack.

Compared to current standard techniques where suspensions are fully linearised and aerodynamic forces are reduced to a fixed load, the proposed approach shows an improvement through a more complete description of the vehicle.

Aerobalance, pitch moment coefficient and pitch moment have been compared in order to define which parameter can better represent the aerodynamic variance. Pitch moment has been found to be the best approach as it uses the pitch moment coefficient multiplied by speed squared. It has also shown how some setup configurations can lead to aerodynamic instability. In that case, the pitch moment statistical variance has been calculated using the pitch moment gain for each track profile. Therefore, the proposed performance index is the integration of the statistical variance of the pitch moment over a specific speed.

A good sensitivity to vehicle parameters variation has been shown to be as expected during track testing. One of the most interesting aspects found in results concerns the possibility of having a vehicle setup which moves aerobalance towards the rear while increasing the pitch moment variance. The front ride height sweep is a good example of this trend.

The proposed method also features the ability to employ different ISO road profiles avoiding the need of measuring track roughness which represents an extra cost for the teams. The index can therefore be valid for a specific track while other standard approaches are not circuit dependent so they are not efficient everywhere.

Finally, it is worth highlighting that the proposed performance index can also be replicated using a special arrangement of a 7-post rig. The air springs must be replaced by spring and dampers that match the stiffness and damping at each trim value.

## Acknowledgements

The authors would like to thank Fortec Motorsport (UK) for supplying raw data and the discussions about the actual 7 post rig results value and utility.

## Disclosure statement

No potential conflict of interest was reported by the authors.

## ORCID

Marco Gadola  <http://orcid.org/0000-0002-5632-590X>

Daniel Chindamo  <http://orcid.org/0000-0003-0902-7472>

## References

- [1] Piola G. Formula 1. 2015–2016 analisi tecnica. Milano (MI): Giorgio Nada Editore; 2016.
- [2] Katz J. Race car aerodynamics: designing for speed. Cambridge (MA): Robert Bentley Publisher; 1995.
- [3] Floyd R, Law E. Simulation and analysis of suspension and aerodynamic interactions of race cars. Motorsport Engineering Conference & Exposition, SAE; 1994.
- [4] Kasprzak JL, Floyd, RS. Use of simulation to tune race car dampers. Motorsport Engineering Conference & Exposition, SAE; 1994.
- [5] Doniselli C, et al. Aerodynamic effects on ride comfort and road holding of automobiles. Veh Syst Dyn. 1996;25(1):99–125.
- [6] Kelly J, Kowalczyk H, Oral H. Track simulation and vehicle characterization with 7 post testing. Motorsport Engineering Conference & Exhibition, SAE; 2002.
- [7] Chindamo D, Gadola M, Marchesin FP. Reproduction of real-world road profiles on a four-poster rig for indoor vehicle chassis and suspension durability testing. Adv Mech Eng. 2017;9(8):1–10.
- [8] New TM. Random road analysis and improved gear ratio selection of a front wheel drive drag racing car [master's thesis]. Clemson University; 2008.
- [9] Barcelo JDP. Optimization of racing car suspensions featuring inerters [dissertation]. Oxford (OX): Oxford Brookes University; 2012.
- [10] Benini C, Gadola M, Chindamo D, et al. The influence of suspension components friction on race car vertical dynamics. Veh Syst Dyn. 2017;55(3):338–350.
- [11] Crema C, Depari A, Flammini A, et al. Smartphone-based system for vital parameters and stress conditions monitoring for non-professional racecar drivers. Proceedings of the 2015 IEEE Sensors. Busn Busan, Korea; 2015.

- [12] Cambiaghi D, Gadola M, Vetturi M. Suspension system testing and tuning with the use of a four-post rig. Motorsport Engineering Conference & Exposition, SAE; 1998.
- [13] Kowalczyk H. Damper tuning with use of a seven post shaker rig. SAE 2002 World Congress. Detroit (MI); 2002.
- [14] Multimatic. A note in the use of four post test rigs; 1998. p. 20.
- [15] MTS System Corporation. RPC Pro Software; 2014.
- [16] Dallara, Formula Renault 3.5 2012 aerobook, release 1.1. Varano de' Melegari (PR): Dallara Automobili; 2012.
- [17] Mavroudakis B. About the simulations of formula 1 racing cars [dissertation]. Stuttgart: University of Stuttgart; 2010.
- [18] Dallara. GP2 2011 aero setup. Varano de' Melegari (PR): Dallara Automobili; 2012.
- [19] Dallara. Dallara F312 manual. Varano de' Melegari (PR): Dallara Automobili; 2012.
- [20] Mygale. Mygale 2008 M08-F3 user manual. Magny Cours (FR): Mygale; 2008.
- [21] Etkin B. Dynamics of atmospheric flight. Mineola (NY): Dover Publications; 2005.
- [22] Molina J, Zhang Z. Aerodynamics of a heaving airfoil in ground effect. AIAA J. 2011;49(6):1168–1179.
- [23] PKM Consulting. SMACBUMP by SMAC user manual. Signes (FR).
- [24] Marchesin FP, Barbosa RS, Alves MAL, et al. Upright mounted pushrod: the effects on race car handling dynamics. 24th International Symposium on Dynamics of Vehicles on Roads and Tracks. Graz, Austria; 2015.
- [25] Dallara. F312 spreadsheet v1.12. Varano de' Melegari (PR): Dallara Automobili; 2013.
- [26] Spinola Barbosa R. Vehicle vibration response subjected to longwave measured pavement irregularity. J Mech Eng Autom. 2012;2(2):17–24.
- [27] Gillespie T. Fundamentals of vehicle dynamics. Michigan (MI): SAE; 1992.